Journal of ELECTRONIC MATERIALS, Vol. 37, No. 11, 2008
DOI: 10.1007/s11664-008-0538-9

Regular Issue Paper

Nanoclay Paste as a Thermal Interface Material for Smooth Surfaces

CHUANGANG LIN[1] and D.D.L. CHUNG[1,2]

1.—Composite Materials Research Laboratory, University at Buffalo, State University of New York, Buffalo, NY 14260-4400, USA. 2.—e-mail: ddlchung@buffalo.edu

A paste in the form of a polyol ester vehicle (liquid) containing 0.6 vol.% nanoclay is an effective thermal interface material. Nanoclay with a high conformability and hence a small bond line thickness is preferred, namely montmorillonite containing a quarternary ammonium salt organic modifier (dimethyl dehydrogenated tallow) at 125 meq/100 g clay, after exfoliation by using the vehicle. When it is used between smooth (0.009 μm) copper surfaces at a pressure of 0.69 MPa, the thermal contact conductance reaches 40×10^4 W/m^2 K, in contrast to the corresponding values of 28×10^4 W/m^2 K, 28×10^4 W/m^2 K, 25×10^4 W/m^2 K, and 24×10^4 W/m^2 K previously reported for carbon black, fumed alumina, fumed zinc oxide, and graphite nanoplatelet pastes. Between rough copper surfaces (12 μm), the conductance provided by the nanoclay paste is slightly below those of the other pastes. The superiority of the nanoclay paste for smooth surfaces is attributed to the submicron bond line thickness; the inferiority for rough surfaces is due to the low thermal conductivity. The conductance provided by the nanoclay paste increases from 31×10^4 W/m^2 K to 40×10^4 W/m^2 K when the pressure is increased from 0.46 MPa to 0.92 MPa. This pressure dependence is stronger than that of any of the other pastes studied.

Key words: Nanoclay, exfoliated clay, thermal paste, thermal interface material, thermal contact, polyol ester, thermal conductance

INTRODUCTION

With the miniaturization and increasing power of microelectronics, heat dissipation has become critical to the performance, reliability, and further miniaturization of microelectronics. A typical thermal solution for a microelectronic system utilizes a thermal interface material (TIM)[1–6] between the die and the heat spreader, and between the heat spreader and the heat sink. The TIM is used to reduce the contact resistance arising from the incomplete contact between two solid surfaces.

Thermal interface materials are mainly in the form of pastes, which are known as thermal pastes.[5–19] A thermal paste comprises a base medium (i.e., the vehicle, which is a liquid) and one or more suspended solid components that includes one that is thermally conductive. Since thermal conductivity has long been assumed in the thermal interface material industry to be the key criterion in determining the effectiveness of a thermal interface material, conventional solid components include various metal and ceramic particles that exhibit high thermal conductivity. Depending on the type of electronic packaging application, an electrically insulating (e.g., ceramic) or electrically conductive (e.g., metallic) solid component may be utilized in TIMs. Alumina, zinc oxide, aluminum nitride, and boron nitride are typical ceramic solid components, while silver and aluminum are the main metallic solid components used in TIMs.

The two solid surfaces involved in a thermal contact are never perfectly flat. There are hills and valleys in the surface topography, thus resulting in air pockets. Since air is a thermal insulator, it is

(Received May 19, 2008; accepted July 29, 2008; published online August 21, 2008)

important to displace the air by using an interface material that conforms to the topography of the mating surfaces. Therefore, conformability is an essential attribute of a thermal interface material. In addition, the spreadability is important, as the thermal resistance increases with the thickness of the TIM. High spreadability results in a small bond line thickness. The conformability and spreadability have recently been shown by Chung et al.[9–17] to be so important that solid components that are not very conductive (e.g., carbon black) can outperform those that are much more conductive (e.g., silver). Nanostructuring helps both conformability and spreadability. The conformability relates to the ability of a nanoscale component such as nanoparticles to fill the microscopic valleys on the proximate surfaces, thereby displacing the air pockets at the interface. In addition, the nanoscale component enables a small bond line thickness, which helps make the thermal resistance low. Nanostructured solid components that have been found to be effective to various degrees include carbon black (CB),[10–14] graphite nanoplatelets (GNP),[15,20] carbon nanotubes,[16] and fumed metal oxides.[17] In particular, GNP is more effective than CB (Cabot) for rough surfaces (15 μm), but is slightly less effective than CB (Cabot) for smooth surfaces (0.009 μm). GNP gives higher thermal conductivity and greater bond line thickness than CB (Tokai or Cabot). In spite of the high thermal conductivity the effectiveness of GNP is limited due to the high bond line thickness.[15] This means that the effectiveness of a thermal paste depends sensitively on both the bond line thickness and the thermal conductivity. A type of nanoplatelet that gives a lower bond line thickness than GNP would be desirable.

Another form of nanoplatelet is nanoclay, as obtained by the exfoliation of clay (such as montmorillonite), which may be organically modified.[21–23] Polymer-nanoclay composites have been extensively studied in various polymer matrices. The results have shown that the dispersal of nanoclay platelets into a matrix improves the physical properties of the matrix, if the platelets are completely exfoliated. The nanoclay addition causes improved toughness, increased tensile strength and flexural strength, and improved barrier properties.[24,25] In relation to TIMs, nanoclay has been used only as a secondary solid component for: (i) disrupting the electrically conductive path so as to make an electrically conductive thermal paste electrically nonconductive,[19] (ii) slowing the diffusion of oxygen and water through the TIM,[26] and (iii) aligning carbon nanotubes in the TIM.[27] In these TIMs containing nanoclay, the primary solid component is one that is relatively high in thermal conductivity (e.g., carbon black[19] and carbon nanotubes[27]). In contrast, due to the nanostructure of nanoclay, the present paper addresses the use of nanoclay as the primary (or sole) solid component in TIMs. In other words, the nanoclay is used in this paper as the thermally conductive component, in the absence of any other component that is more conductive.

The objectives of this paper are (i) to evaluate the effectiveness of nanoclay as the sole solid component in TIMs, (ii) to compare the effectiveness of nanoclay with those of competing solid components, and (iii) to evaluate the relative effectiveness of various types of organic modification to nanoclay for this application. Thus, both the formulation and the performance of the nanoclay thermal pastes are addressed.

EXPERIMENTAL METHODS

Materials

This section describes the formulation of thermal pastes. The vehicle consists of polyol esters, which are attractive for their ability to resist elevated temperatures. The polyol esters used were pentaerythritol ester of linear and branched fatty acids and dipentaerythritol ester of linear and branched fatty acids. The polyol ester mixture was Hatcol 2372, as provided by Hatco Corp., Fords, NJ.[12] The specific gravity was 0.97.

The nanoclay (exfoliated clay) was obtained by subjecting the clay to an exfoliation-adsorption process.[27–33] It was used in amounts ranging from 0.1 vol.% to 5.0 vol.% of the resulting paste. Three types of organic modified clay (i.e., organoclay), namely Cloisite 10A, Cloisite 25A, and Cloisite 15A, were provided by Southern Clay Products, Inc., Gonzales, TX. The clay was a natural montmorillonite (di-octahedral, in the smectite family) phyllosilicate intercalated with an organic modifier, namely a quaternary ammonium salt, which was at a concentration of 95–125 meq/100 g clay. (The charge on the unmodified montmorillonite was 92 meq/100 g clay.) Prior to the exfoliation-adsorption process, the particle size was such that 10% was less than 2 μm, 50% was less than 6 μm, and 90% was less than 13 μm. After exfoliation, the clay (known as nanoclay) was made of layered magnesium aluminum silicate platelets that were 1 nm thick and 70 nm to 150 nm across, with an aspect ratio of 70 to 150 and a surface area exceeding 750 m^2/g. Phyllosilicates are inherently hydrophilic, but ion exchange involving the cations in the silicate and the ammonium salt renders the clay more hydrophobic. The modified clay has a reduced surface energy, which is well suited for use with organic matrices. Cloisite 10A was modified by dimethyl benzyl hydrogenated tallow, a quaternary ammonium salt at a concentration of 125 meq/100 g clay; Cloisite 15A was modified by dimethyl dehydrogenated tallow, a quaternary ammonium salt at 125 meq/100 g clay; Cloisite 25A was modified by dimethyl hydrogenated tallow, a 2-ethylhexyl quaternary ammonium salt at a concentration of 95 meq/100 g clay.

The exfoliation–adsorption processing process[28–34] combines exfoliation (separation of the silicate

platelets) and adsorption (adsorption of an organic material, i.e., the vehicle of the thermal paste, on the surface of the platelets). This process involves dissolving the polyol ester vehicle in a solvent, which is chlorobenzene (Mallinckrodt Baker Inc., Phillipsburg, NJ, with assay 100.0% and specific gravity 1.11).[29] Interaction of the solution with the ammonium salt used to modify the clay, along with sonication,[29] causes exfoliation of the silicate and adsorption of the polyol ester solution on the exfoliated silicate platelets. Sonication was conducted by using a 100-W ultrasonic cleaner (Fisher Scientific International Inc., FS60H, Hampton, NH). Subsequent evaporation of the solvent allowed the vehicle to adsorb onto the exfoliated silicate layers, thereby rendering a nanocomposite.

The specific procedure of the exfoliation–adsorption process of this work is described below. The solvent and clay were mixed in a 70:1 mass ratio and vigorously hand mixed to fully disperse the clay in the solvent. The clay dispersion was then placed in a water bath in the ultrasonic cleaner and sonicated for 2 h. Next the vehicle was added, vigorously hand mixed to achieve a homogeneous dispersion, and then sonicated for an additional 15 min. During sonication, the temperature of the water bath was held between 35°C and 45°C. A large portion of the solvent was then removed by evaporation using a hot plate held at 100°C for 4 h. Any remaining solvent was then removed by placing the samples in a vacuum chamber and heating to 85°C for 24 h.

The thermal pastes were prepared by mixing, followed by placing the paste in a vacuum chamber (which involves a mechanical vacuum pump) for the purpose of solvent removal.

Testing

Thermal Contact Conductance and Thermal Conductivity Measurements

A steady-state method known as the guarded hot plate method (ASTM method D5470) is used to measure the thermal contact conductance for various thermal contacts. In this method, various thermal pastes are sandwiched between the 1 inch × 1 inch (25 mm × 25 mm) proximate surfaces of two copper blocks (both 1 mm × 1 inch surfaces of each block having a controlled degree of roughness). Each copper block has a height of 35 mm.

The heat in this test is provided by a 3 inch × 3 inch (76 mm × 76 mm) copper block that has two embedded heating coils (the top block in Fig. 1). During the period of temperature rise, the heating rate is controlled to 3.2°C/min by using a temperature controller. This copper block is in contact with one of the 1 inch × 1 inch copper blocks that sandwich the thermal interface material. The cooling in this test is provided by a second 3 inch × 3 inch copper block, which is cooled by running water that flows into and out of the block (the bottom block in Fig. 1). This block is in contact with the other of the two 1 inch × 1 inch copper blocks that sandwich the thermal paste. The two mating surfaces of the two 1 inch × 1 inch copper blocks are either "rough" (12 μm roughness, as attained by mechanical polishing) or "smooth" (0.009 μm roughness and 0.040 μm to 0.116 μm flatness, as attained by diamond turning). A 100-Ω resistance temperature detector (RTD) probe was inserted into four holes (A, B, C, and D in Fig. 1, each of diameter 3.2 mm). Two of the four holes are located in each of the 1 inch × 1 inch copper blocks. The temperature gradient is determined from $T_1 - T_2$ and $T_3 - T_4$, where the temperatures T_1, T_2, T_3, and T_4 are measured at holes A, B, C, and D respectively. The quantities $T_1 - T_2$ and $T_3 - T_4$ should be equal at equilibrium, which is attained after holding the temperature of the heater at the desired value for 30 min. Equilibrium is assumed when the temperature variation is within ±0.1°C for a period of 15 min. At equilibrium, the temperature of the hot block is in the range of 70°C to 80°C, that of the cold block is in the range of 60°C to 40°C, while that of the thermal paste is in the range of 60°C to 70°C. The pressure in the direction perpendicular to the plane of the thermal interface is controlled by using a hydraulic press at pressures of 0.46 MPa, 0.69 MPa, and 0.92 MPa. This pressure range is within the range that is used in the TIM industry. The system is thermally insulated by wrapping laterally all the copper blocks with glass-fiber cloth.

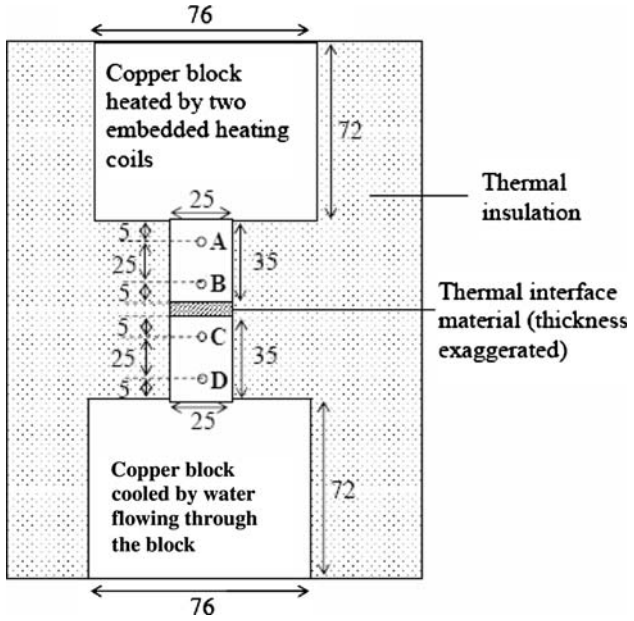

Fig. 1. A schematic representation of the steady-state method (guarded hot plate method) of thermal contact conductance measurement. A, B, C, and D in the drawing are holes of diameter 2.4 mm, corresponding to temperatures T_1, T_2, T_3, and T_4, respectively. A thermocouple (type T) is inserted into each hole. All dimensions are in millimeters.

In accordance with ASTM method D5470, the heat flow Q is given by

$$Q = \frac{\lambda A}{d_A}\Delta T \tag{1}$$

where $\Delta T = T_1 - T_2 = T_3 - T_4$, λ is the thermal conductivity of copper, A is the area of the 1 inch × 1 inch copper block, and d_A is the distance between thermocouples T_1 and T_2 (i.e., 25 mm).

The temperature at the top surface of the thermal interface material is T_A, which is given by

$$T_A = T_2 - \frac{d_B}{d_A}(T_1 - T_2), \tag{2}$$

where d_B is the distance between thermocouple T_2 and the top surface of the thermal interface material (i.e., 5 mm). The temperature at the bottom surface of the thermal interface material is T_D, which is given by

$$T_D = T_3 + \frac{d_D}{d_C}(T_3 - T_4), \tag{3}$$

where d_D is the distance between thermocouple T_3 and the bottom surface of the thermal interface material (i.e., 5 mm) and d_C is the distance between thermocouples T_3 and T_4 (i.e., 25 mm).

The thermal resistivity θ is given by

$$\theta = (T_A - T_D)\frac{A}{Q} \tag{4}$$

Note that insertion of Eq. 1 into Eq. 4 causes cancellation of the term A, so that θ is independent of A. The thermal contact conductance is the reciprocal of θ.

The thermal conductivity within a thermal paste is to be distinguished from the thermal contact conductance across a thermal contact. This thermal conductivity measurement was also based on the ASTM D5470 method, as described in Ref. 15. The thermal conductivity of selected thermal pastes are measured by using this method, with four spacers to control the paste thickness.

The thermal resistance of a system consisting of a thermal paste sandwiched between a heat source and a heat sink can be simply modeled by thermal resistances in series. Thus,

$$R = \frac{h}{kA} + R_1 + R_2 \tag{5}$$

where A is the geometric area of the contact, h is the bond line thickness, k is the thermal conductivity of the thermal paste, R (in units of K/W) is the total thermal resistance of the sandwich, and R_1 and R_2 are the interfacial resistances of the interface between the thermal paste and the two surfaces that sandwich the paste. The geometric area is the flat contact area and is to be distinguished from the true area, which reflects the interface area associated with the roughness of each of the proximate surfaces. The total thermal resistivity of the sandwich is RA (in units of m^2 K/W). The inverse of the thermal resistivity is the thermal contact conductance (in units of W/m^2 K).

The thermal conductivity k is determined by measuring the thermal resistivity RA for various values of the thermal paste thickness h. The plot of RA versus h is linear, with slope $1/k$ and intercept $(R_1 + R_2)$ A at the vertical axis, as indicated by Eq. 5. The product R_1A is the geometric interfacial resistivity of the interface between the thermal paste and one of the two proximate surfaces, while the product R_2A is the geometric interfacial resistivity of the interface between the thermal paste and the other proximate surface.

Viscosity Measurement

The viscosity describes the resistance to shear deformation. It is a commonly used attribute for describing pastes. The viscosity of various pastes was measured by using a viscometer (Brookfield Engineering Laboratories, Inc., Middleboro, MA, Model LVT Dial-Reading Viscometer, with Model SSA-18/13R Small Sample Adaptor). In addition, the viscometer was used to measure the shear thinning index and the thixotropic index, as explained below.

Materials whose viscosities respond to a shear force by either increasing or decreasing as the shear rate increases are said to be non-Newtonian. This effect is known as shear thickening (in case of the viscosity increasing) or shear thinning (in case of the viscosity decreasing). To calculate the shear thinning index, one measures the viscosity at a low shear rate (i.e., a low number of revolutions per minute) and at a rate that is ten times higher. The ratio of the viscosity at the low rate divided by the viscosity at the high rate is called the shear thinning index. This index indicates the scale of shear thinning for a material within the range of rotational speed.[32] The higher this ratio, the greater the shear thinning. This paper uses a range of speed from 0.3 rpm to 3 rpm to study the effect of clay content on shear thinning.

Thixotropy refers to the rheological behavior in which a material flows only under a stress. An example of a thixotropic paste is ketchup. The thixotropic index is a time-dependent rheological property that describes the extent of thixotropic behavior. A range of rotational speeds are selected. The apparent viscosity is measured while the shear rate is progressively increased to the maximum and then progressively decreased to the minimum at constant time intervals. After the last viscosity measurement, the viscometer is turned off for 10 min. After this rest period, a measurement of the viscosity at the lowest rate is taken again. Two methods can be used to calculate the thixotropic index. Method A uses the ratio of the increasing

speed viscosity to that of the decreasing speed viscosity. Method B uses the ratio of the lowest speed viscosity taken after the rest period to that before the rest period. Method A was used to measure the thixotropic index in this study. For both methods, the higher the ratio, the greater the thixotropy.[33]

Conformability Measurement

A penetration testing method has been previously modified[12] to measure the conformability of the pastes. High conformability corresponds to a large penetration depth. In this study, the same method is used to measure the penetration depth of various pastes, except that the test durations used include 3 s and 5 s in order to widen the range of specimens that can be tested (in contrast to the duration of 5 s used in previous work[12]) and a smaller specimen container diameter (15 mm, in contrast to the diameter of 35 mm in prior work,[12] in order to reduce the amount of specimen required) is used.

Bond Line Thickness Measurement

The dependence of the bond line thickness of a thermal paste on the pressure was measured by using an indirect method in which the bond line thickness is calculated from the controlled volume of the paste and the measured area of the paste after the spreading associated with its being sandwiched by the copper blocks (those used for thermal contact conductance measurement in the case of smooth surfaces) at a controlled load (provided by a constant weight) for 1 min. The paste is applied to the center of the surface of one of the copper blocks prior to bringing the two blocks together and subsequent compression, which causes the paste to spread. After the compression, the blocks are separated and the diameter of the spread paste is measured. The area of the spread paste is calculated from the measured diameter of the spread paste, as the area is essentially circular. The pressure of the compression is calculated from the constant weight and the area covered by the spread paste. By using different volumes of thermal paste, different areas are covered by the spread paste and the pressure on the paste is varied, thereby allowing investigation of the dependence of bond line thickness on pressure. The pressure range is similar to that used for thermal contact conductance measurement.

RESULTS AND DISCUSSION

Thermal Contact Conductance

The thermal contact conductance was measured for various combinations of nanoclay type, nanoclay volume fraction, copper surface smoothness, and contact pressure. Figures 2 and 3 show the values for smooth surfaces at pressures of 0.46 MPa and 0.69 MPa, respectively. The results in Figs. 2 and 3 and Table I show that, for the same range of nanoclay volume fraction, the pastes containing Cloisite 15A nanoclay give higher thermal conductance

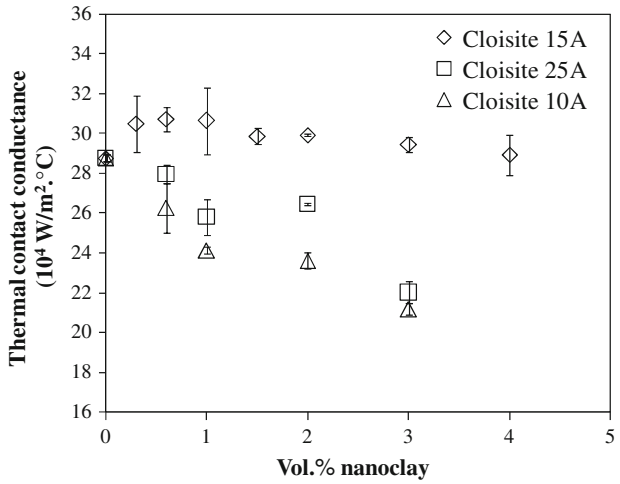

Fig. 2. Effect of the type and volume fraction of nanoclay on the thermal contact conductance of nanoclay thermal pastes between smooth surfaces at 0.46 MPa. ◇: Cloisite 15A nanoclay, □: Cloisite 25A nanoclay, Δ: Cloisite 10A nanoclay.

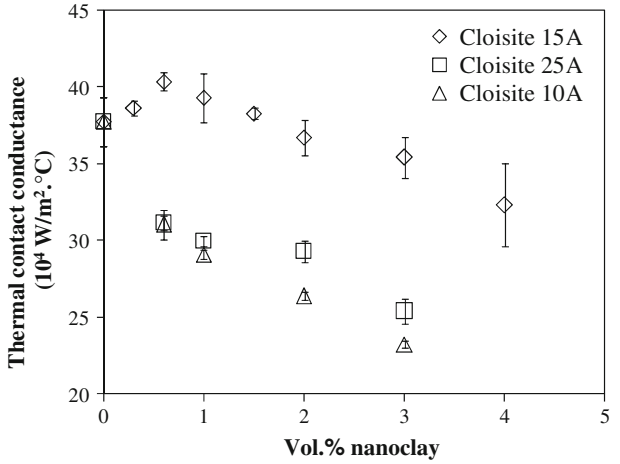

Fig. 3. Effect of the type and volume fraction of nanoclay on the thermal contact conductance of nanoclay thermal pastes between smooth surfaces at 0.69 MPa. ◇: Cloisite 15A nanoclay, □: Cloisite 25A nanoclay, Δ: Cloisite 10A nanoclay.

than the pastes containing Cloisite 10A nanoclay or Cloisite 25A nanoclay. The thermal conductance is increased relative to the case of the vehicle without any solid component by the addition of Cloisite 15A nanoclay in amounts up to 0.6 vol.%, but is slightly decreased from this maximum value upon further increase of the nanoclay volume fraction. In contrast, the thermal conductance of the pastes with Cloisite 10A nanoclay and Cloisite 25A nanoclay decrease monotonically and quite significantly with increasing nanoclay volume fraction. At 0.46 MPa, the highest thermal conductance of around 30×10^4 W/m^2 °C was attained with 0.3 vol.% to 1.0 vol.% Cloisite 15A nanoclay. At 0.69 MPa, the highest thermal conductance of 40×10^4 W/m^2 °C was attained with 0.6 vol.% Cloisite 15A nanoclay.

Figure 4 shows the thermal contact conductance of the Cloisite 15A nanoclay pastes tested between

Table I. Thermal Contact Conductance and Bond Line Thickness for Various Thermal Pastes, as Measured Between Copper Surfaces (Either Rough or Smooth) at Various Pressures (0.46 MPa to 0.92 MPa)

Solid Component		Thermal Contact Conductance (10^4 W/m^2 K)				
		Rough Surfaces			Smooth Surfaces	
Type	Vol.%	0.46 MPa	0.69 MPa	0.92 MPa	0.46 MPa	0.69 MPa
None	0.0	10.50 ± 0.60	10.70 ± 0.10	11.30 ± 0.20	28.79 ± 0.16	32.72 ± 1.62
Cloisite 15A nanoclay	0.3	—	—	—	30.51 ± 1.41	38.62 ± 0.50
Cloisite 15A nanoclay	0.6	—	—	—	30.74 ± 0.62	40.35 ± 0.59
Cloisite 15A nanoclay	1.0	7.87 ± 0.05	8.50 ± 0.25	8.95 ± 0.10	30.66 ± 1.69	39.30 ± 1.60
Cloisite 15A nanoclay	1.5	8.80 ± 0.11	8.88 ± 0.13	9.13 ± 0.07	29.90 ± 0.39	38.26 ± 0.38
Cloisite 15A nanoclay	2.0	9.01 ± 0.13	9.51 ± 0.07	9.87 ± 0.05	29.95 ± 0.06	36.68 ± 1.18
Cloisite 15A nanoclay	3.0	8.21 ± 0.12	9.45 ± 0.03	9.78 ± 0.16	29.47 ± 0.38	35.41 ± 1.34
Cloisite 15A nanoclay	4.0	7.69 ± 0.11	8.60 ± 0.16	8.76 ± 0.07	28.95 ± 1.02	32.29 ± 2.71
Cloisite 25A nanoclay	0.6	—	—	—	27.99 ± 0.49	31.12 ± 0.46
Cloisite 25A nanoclay	1.0	—	—	—	25.82 ± 0.89	29.95 ± 0.33
Cloisite 25A nanoclay	2.0	—	—	—	26.47 ± 0.06	29.29 ± 0.69
Cloisite 25A nanoclay	3.0	—	—	—	22.03 ± 0.56	25.40 ± 0.80
Cloisite 10A nanoclay	0.6	—	—	—	26.27 ± 1.26	31.04 ± 0.95
Cloisite 10A nanoclay	1.0	—	—	—	24.16 ± 0.16	29.07 ± 0.31
Cloisite 10A nanoclay	2.0	—	—	—	23.63 ± 0.39	26.37 ± 0.25
Cloisite 10A nanoclay	3.0	—	—	—	21.19 ± 0.29	23.22 ± 0.24
Carbon black[a]	2.4	9.70 ± 0.11	10.23 ± 0.11	11.79 ± 0.27	25.91 ± 0.16	27.75 ± 0.14
Alumina[b]	2.4	10.00 ± 0.24	10.55 ± 0.28	10.52 ± 0.27	25.13 ± 0.76	27.76 ± 0.25
Zinc oxide[c]	4.0	10.10 ± 0.20	10.80 ± 0.22	11.12 ± 0.26	20.30 ± 0.17	25.22 ± 0.87
GNP[15]	2.4	11.72 ± 0.28	11.98 ± 0.18	12.36 ± 0.10	22.07 ± 1.18	24.47 ± 0.37
Ceramique[11]	–	7.21 ± 0.10	8.47 ± 0.53	9.92 ± 0.41	21.48 ± 1.12	24.10 ± 0.76
Shin-Etsu[17]	–	7.76 ± 0.14	8.43 ± 0.20	8.78 ± 0.11	19.87 ± 0.27	22.55 ± 0.43

GNP = graphite nanoplatelet; [a]Vulcan XC72R (Cabot Corp., Billerica, MA), 2.4 vol.%[11]; [b]Fumed alumina with silane coating, Aeroxide ALU C 805, Degussa AG (Hanau, Germany), 2.4 vol.%[17]; [c]Fumed zinc oxide with silane coating, Z805, Degussa AG (Hanau, Germany), 4.0 vol.%.[17]

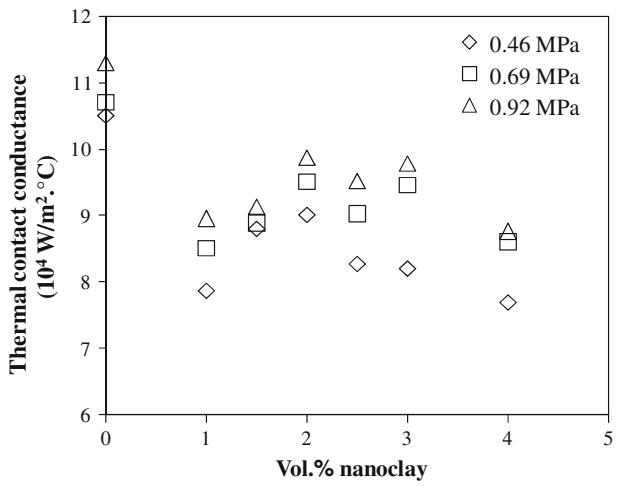

Fig. 4. Effect of volume fraction of Cloisite 15A nanoclay on thermal contact conductance of nanoclay thermal pastes between rough surfaces at various pressures. ◇: 0.46 MPa, □: 0.69 MPa, Δ: 0.92 MPa.

rough surfaces at 0.46 MPa, 0.69 MPa, and 0.92 MPa. An abrupt drop in thermal conductance occurs upon the addition of 1 vol.% Cloisite 15A nanoclay to the vehicle. In contrast, the conductance is increased upon the addition of a small volume fraction of Cloisite 15A nanoclay in the smooth case (Figs. 2 and 3).

In the rough case, Fig. 4 also shows that an increase of the nanoclay volume fraction from 1 vol.% to the range between 2 vol.% and 3 vol.% increases the thermal conductance. This is probably because of the increase in the thermal conductivity within the paste as the nanoclay content increases. However, increase of the nanoclay volume fraction beyond 2 vol.% to 3 vol.% decreases the thermal conductance, probably because of the increased viscosity and the consequent decrease in spreadability and increase in the bond line thickness. In other words, a compromise between thermal conductivity and bond line thickness is required for attaining a high thermal contact conductance, as discussed further in the "Conformability" section.

For the Cloisite 15A nanoclay paste, the optimum nanoclay volume fraction is 0.6% for smooth surfaces; this volume fraction is slightly more effective than 0.3 vol.% or 1.0 vol.%. For rough surfaces, the optimum volume fraction is 2.0 vol.%, with 1.5 vol.% and 3.0 vol.% being slightly less effective.

Table I shows a compilation of the data obtained in this study and those of previous studies

conducted by Chung et al.[11,15,17] using the same testing method. In the case of rough surfaces, Cloisite 15A nanoclay is not as effective as carbon black, alumina, zinc oxide or GNP. However, in the case of smooth surfaces, Cloisite 15A nanoclay is more effective than any of these four. This is because the rough surface has deeper valleys than the smooth surface, thus resulting in the need for heat to go through a relatively longer distance within the paste. As a consequence, the thermal conductivity within the paste is more important for the rough case than the smooth case. GNP,[15] carbon black,[35] alumina, and zinc oxide[36] are more thermally conductive than nanoclay,[37] thus causing these pastes to outperform the nanoclay pastes in the rough case. Further discussion on thermal conductivity is provided in the "Conformability" section. In the smooth case, Cloisite 15A nanoclay is most effective, presumably due to the high spreadability associated with the nanoplatelet morphology of the nanoclay. Due to the interlayer interaction of graphite (as indicated by the AB stacking sequence in the crystal structure of graphite), the nanoplatelet is probably thicker for GNP than nanoclay.

At least for the smooth case, an increase of pressure from 0.46 MPa to 0.92 MPa significantly increases the effectiveness of the nanoclay pastes, particularly when the nanoclay contains Cloisite 15A at a relatively low volume fraction. For example, for the paste containing 0.6 vol.% Cloisite 15A nanoclay, the conductance increases from 31 W/m^2 K to 40 W/m^2 K when the pressure is increased from 0.46 MPa to 0.69 MPa. In contrast, for the carbon black paste of prior work,[11] the conductance increases from 26 W/m^2 K to only 28 W/m^2 K when the pressure is increased from 0.46 MPa to 0.69 MPa; for the alumina paste of prior work,[17] the conductance increases from 25 W/m^2 K to only 28 W/m^2 K when the pressure is increased from 0.46 MPa to 0.69 MPa (Table I). The relatively strong pressure dependence of the nanoclay pastes is attributed to the relatively high spreadability.

In the rough case, the conductance increases slightly with increasing pressure for all the pastes studied (Table I). For the nanoclay pastes, the pressure dependence is much stronger for the smooth case than the rough case. For example, for the paste containing 1.0 vol.% Cloisite 15A nanoclay, the conductance increases from 31×10^4 W/m^2 K to 39×10^4 W/m^2 K when the pressure is increased from 0.46 MPa to 0.69 MPa in the smooth case, but increases from 7.9×10^4 W/m^2 K to 8.5×10^4 W/m^2 K when the pressure is increased from 0.46 MPa to 0.69 MPa in the rough case. This difference in the degree of pressure dependence between the smooth and rough cases is because the spreadability affects the conductance more in the smooth case than in the rough case.

In the smooth case, the conductance decreases with increasing nanoclay volume fraction beyond the optimum volume fraction more significantly at 0.69 MPa (Fig. 3) than at 0.46 MPa (Fig. 2). This is because the spreadability is diminished upon increasing the nanoclay volume fraction and the spreadability shows its influence more when the pressure is higher.

Upon comparison with commercial thermal pastes, namely Ceramique and Shin-Etsu, the Cloisite 15A nanoclay paste is superior both in the rough and smooth cases (Table I). This is due to the high conformability and spreadability of the Cloisite 15A nanoclay paste compared with these commercial pastes.

All values of the thermal contact conductance reported in this work (Table I) are much higher than the highest value of 8×10^3 W/m^2 K that had been previously reported for both an aligned multiwalled carbon nanotube (0.4 vol.%) array and a nonaligned dispersed multiwalled carbon nanotube (0.4 vol.%) silicone-matrix composite.[38]

Thermal Conductivity

Table II shows that the thermal conductivity is comparable for nanoclay, carbon black, and alumina pastes. The value is higher for the zinc oxide paste and even higher for the GNP paste. This means that the high thermal contact conductance attained by the nanoclay paste for the smooth case (Table I) is not due to the thermal conductivity of the nanoclay. Although the thermal conductivity of the GNP paste is about four times that of the Cloisite 15A nanoclay (1.0 vol.%) paste, its bond line thickness (1.2 μm to 1.5 μm) is four to six times that of the nanoclay paste at the same pressure of 0.4 MPa to 0.9 MPa (Fig. 9). This explains why the GNP paste is inferior to the nanoclay paste in terms of the thermal contact conductance for smooth surfaces, even though it has a much higher thermal conductivity. The bond line thickness of the pastes studied is further discussed in the "Viscosity" section.

A similar situation applies to aligned carbon nanotube (CNT) arrays grown by chemical vapor deposition on silicon substrates.[38] In spite of the relatively high value of the thermal conductivity of the carbon nanotube array (1.21 W/m K,[38] about 10 times higher than that of 1.0 vol.% Cloisite 15A), the large bond line thickness of 0.1 mm or above (about 50 times higher than that of 1.0 vol.% Cloisite 15A) limits the effectiveness of the array as a thermal interface material.

Schelling et al.[39] considered the use of an aligned CNT film as a TIM. They measured the TIM thermal conductivity, but did not measure the thermal contact conductance across the thermal contact. Without the latter, the performance of the material as a TIM is unclear.

Viscosity

In a dispersion comprising particles and a vehicle and subjected to a shear stress (as provided by a viscometer), the interaction between particles and that between particles and the vehicle govern the

Table II. Thermal Conductivity and Geometric Interfacial Thermal Resistivity of Selected Pastes under No Load

Filler	Vol.%	Linear fit of the Dependence of the Thermal Resistivity (y) on the Bond Line Thickness (x) (Fig. 4 of Ref. 15)	Thermal Conductivity (W/m K)
Cloisite 15A nanoclay	0	$y = 8.386\,x + 2.4 \times 10^{-6}$, $R^2 = 0.999$	0.119 ± 0.001
Cloisite 15A nanoclay	1	$y = 8.345\,x + 5.3 \times 10^{-5}$, $R^2 = 0.998$	0.120 ± 0.002
Cloisite 15A nanoclay	4	$y = 7.483\,x - 1.66 \times 10^{-5}$, $R^2 = 0.998$	0.134 ± 0.001
Carbon black[a]	2.4	$y = 7.785\,x + 1.1 \times 10^{-5}$, $R^2 = 0.997$	0.128 ± 0.001
Alumina[b]	2.4	$y = 8.145\,x + 2.4 \times 10^{-5}$, $R^2 = 0.999$	0.123 ± 0.002
Zinc oxide[c]	4	$y = 6.566\,x + 9.2 \times 10^{-6}$, $R^2 = 0.997$	0.152 ± 0.002
GNP[15]	2.4	$y = 2.103\,x + 6.2 \times 10^{-6}$, $R^2 = 0.999$	0.476 ± 0.005

[a]Vulcan XC72R (Cabot Corp., Billerica, MA), 2.4 vol.%[11]; [b]Fumed alumina with silane coating, Aeroxide ALU C 805, Degussa AG (Hanau, Germany), 2.4 vol.%[17]; [c]Fumed zinc oxide with silane coating, Z805, Degussa AG (Hanau, Germany), 4.0 vol.%.[17]

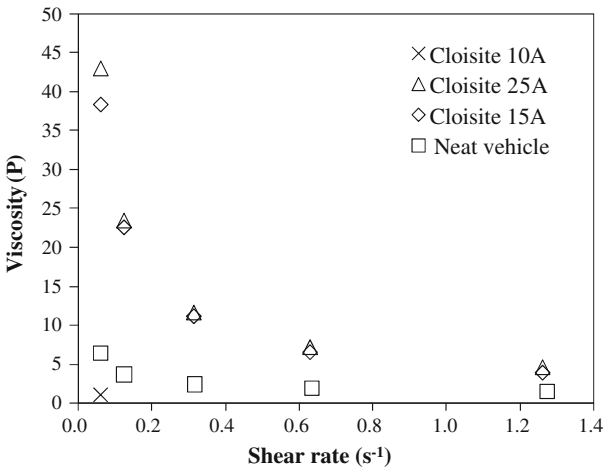

Fig. 5. Effect of shear rate on the viscosity for different types of paste with 0.6 vol.% nanoclay. ×: Cloisite 10A nanoclay, Δ: Cloisite 25A nanoclay, ◇: Cloisite 15A nanoclay, □: Neat vehicle.

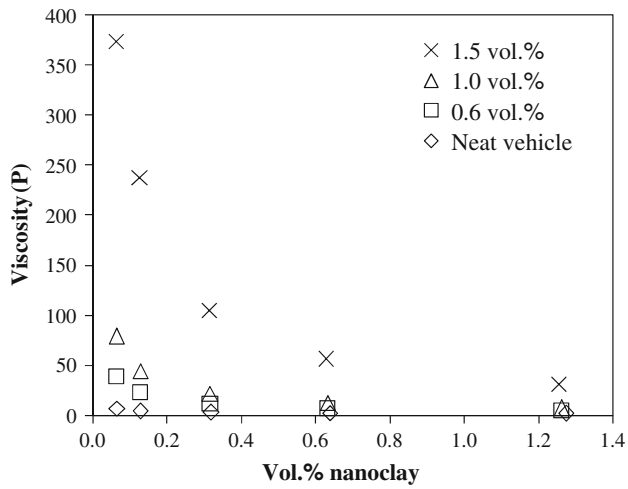

Fig. 6. Effect of the clay volume fraction on the viscosity for Cloisite 15A nanoclay. ×: 1.5 vol.%, Δ: 1.0 vol.%, ◇: 0.6 vol.%, □: Neat vehicle.

viscosity of the dispersion. The viscosity of the three types of nanoclay at 0.6 vol.% is shown in Fig. 5. The viscosity of the Cloisite 10A nanoclay paste has the highest viscosity among the three types of nanoclay pastes; the viscosity of the Cloisite 25A nanoclay paste is close to that of the Cloisite 15A nanoclay paste. According to Southern Clay Products Co.,[40] the surface hydrophobicity of the nanoclay increases in the order: Cloisite 10A, Cloisite 25A, Cloisite 15A. Since Cloisite 15A nanoclay has higher surface hydrophobicity, it has greater affinity with the organic vehicle, which is an oil. As a result, Cloisite 15A nanoclay gives a relatively low viscosity.

The viscosity increases as the Cloisite 15A nanoclay volume fraction increases, as shown in Fig. 6. The difference is particularly large between 1.0 vol.% and 1.5 vol.%. This is probably because 1.5 vol.% is close to the gel point.[41]

The viscosities of previously developed thermal pastes, i.e., carbon black paste, alumina paste, and zinc oxide paste, and that of the Cloisite 15A nanoclay paste of this work are compared in Fig. 7. Based on intuition, a low viscosity is expected to be valuable for attaining a high conductance for the case of smooth surfaces. The nanoclay paste has a lower viscosity than the carbon black paste (Fig. 7)

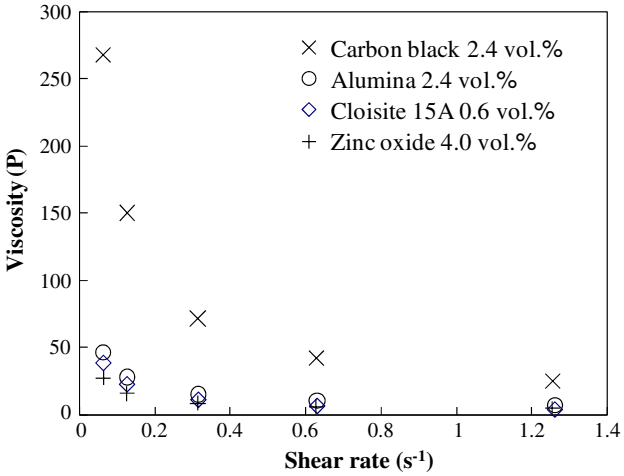

Fig. 7. Effect of shear rate on the viscosity for pastes with various solid components. ×: 2.4 vol.% carbon black (Vulcan XC72R, Cabot Corp., Billerica, MA[11]); ○: 2.4 vol.% silane treated fumed alumina (Aeroxide ALU C 805, Degussa AG, Hanau, Germany[17]); ◇: 0.6 vol.% Cloisite 15A nanoclay, +: 4.0 vol.% silane treated fumed zinc oxide (Z805, Degussa AG, Hanau, Germany[17]).

Table III. Shear Thinning Index and Thixotropic Index of Various Pastes

Nanoclay	Vol.%	Shear Thinning Index	Thixotropic Index
None	0	3.45 ± 0.22	1.35 ± 0.01
Cloisite 10A	0.6	6.55 ± 0.44	0.80 ± 0.13
Cloisite 25A	0.6	6.03 ± 0.22	1.09 ± 0.14
Cloisite 15A	0.6	5.89 ± 0.11	1.08 ± 0.11
Cloisite 15A	1.0	6.50 ± 0.01	1.01 ± 0.01
Cloisite 15A	1.5	7.40 ± 0.02	0.79 ± 0.10

and indeed gives higher conductance than the carbon black paste for the smooth case (Table I). However, the alumina paste and the zinc oxide paste have similar viscosities to the nanoclay paste (Fig. 7), but give lower conductance than the nanoclay paste for the smooth case (Table I). Thus, there is no correlation between the viscosity and the thermal contact conductance.

For all the nanoclay pastes in this study, the viscosity decreases with increasing shear rate, indicating shear thinning. The shear thinning index is shown in Table III. When compared at 0.6 vol.%, Cloisite 10A nanoclay has the highest shear thinning index, while Cloisite 25A and Cloisite 15A nanoclays are similar in terms of this index. For Cloisite 15A nanoclay, the index increases with increasing nanoclay content. This is due to the increasing degree of alignment of the nanoclay platelets as the shear rate increases. The index has been previously reported to increase upon the addition of fumed alumina.[17]

The thixotropic index is shown in Table III. For Cloisite 15A nanoclay pastes, this index is lower at 1.5 vol.% than at the lower volume fractions. This is consistent with our previous report that this index decreases monotonically with increasing Cloisite 25A nanoclay content.[19] This decrease is believed to be due to the nonclassical thixotropy of montmorillonite clay suspensions.[33] This behavior is associated with a slow recovery process after the application of shear, although the breakdown upon shear is rapid.

Table IV. Conformability (As Indicated by Depth of Penetration) of Various Thermal Pastes

Solid Component	Penetration Depth (mm)
2.4 vol.% carbon black[a,c]	16.7 ± 5.1
2.4 vol.% alumina[a,d]	31.8 ± 3.9
4.0 vol.% zinc oxide[a,e]	58.2 ± 0.8
0.6 vol.% Cloisite 15A nanoclay[a]	53.8 ± 0.3
0.6 vol.% Cloisite 25A nanoclay[a]	46 ± 4
0.6 vol.% Cloisite 10A nanoclay[a]	38 ± 2
3.0 vol.% Cloisite 15A nanoclay[b]	5.0 ± 0.3
3.0 vol.% Cloisite 25A nanoclay[b]	2.7 ± 0.3
3.0 vol.% Cloisite 10A nanoclay[b]	2.1 ± 0.6

[a]Test duration: 3 s; [b]Test duration: 5 s; [c]Vulcan XC72R (Cabot Corp., Billerica, MA)[11]; [d]Silane teated fumed alumina, Aeroxide ALU C 805, Degussa AG (Hanau, Germany)[17]; [e]Silane treated fumed zinc oxide, Z805, Degussa AG (Hanau, Germany).[17]

Conformability

The conformability is higher for the Cloisite 15A nanoclay (0.6 vol.%) paste than for the alumina paste or the carbon black paste (Table IV), while the conductance for the smooth case is higher for the nanoclay paste than for the alumina or the carbon black paste. The conformability is comparable for the nanoclay paste and the zinc oxide paste, in spite of the substantially higher thermal contact conductance provided by the former for the smooth case (Table I). Table IV also shows that the conformability is higher for the zinc oxide paste than for the alumina paste or the carbon black paste. However, the conductance is lower for the zinc oxide paste than for the alumina or carbon black paste (Table I). Cloisite 10A nanoclay at 3.0 vol.% gives much lower conformability than zinc oxide at 4.0 vol.% (Table IV), but the two give similar values for the thermal contact conductance (Table I). These observations mean that a high thermal contact conductance does not correlate well with a high conformability.

Among the nanoclay pastes with various types of nanoclay at various volume fractions, the correlation between conformability and thermal contact conductance is evident. The conformability decreases in the order: Cloisite 15A, Cloisite 25A, Cloisite 10A (Table IV); the conductance is highest for Cloisite 15A (Table IV). For each type of nanoclay, the conformability decreases with increasing

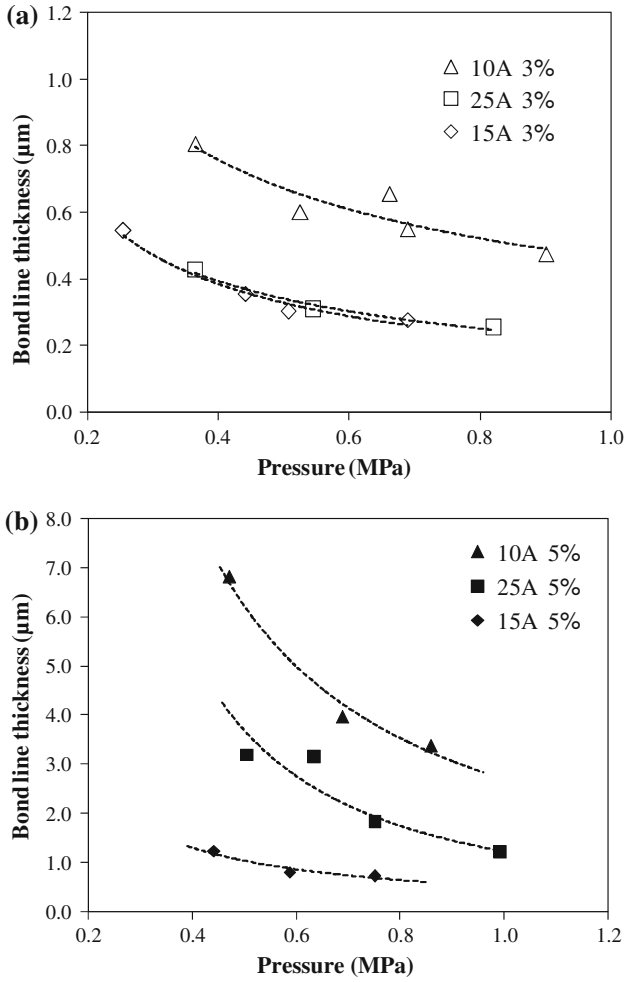

Fig. 8. Dependence of the bond line thickness on the pressure of various pastes. (a) 3.0 vol.% clay, △: Cloisite 10A nanoclay, □: Cloisite 25A nanoclay, ◇: Cloisite 15A nanoclay; (b) 5.0 vol.% clay, ▲: Cloisite 10A nanoclay, ■: Cloisite 25A nanoclay, ◆: Cloisite 15A nanoclay.

nanoclay volume fraction from 0.6% to 3.0% (Table IV); the conductance also decreases with increasing nanoclay volume fraction from 0.6% to 3.0% (Table I).

Bond Line Thickness

The bond line thickness of the pastes with 3.0 vol.% and 5.0 vol.% of each of the three types of nanoclay was measured by the method described in the "Bond Line Thickness Measurement" section. Figure 8a shows the dependence of the bond line thickness on pressure for pastes with Cloisite 10A, Cloisite 25A, and Cloisite 15A nanoclays, each at 3.0 vol.%. The bond line thickness of pastes with all three types of nanoclay is in the submicron range, such that Cloisite 10A nanoclay has a higher bond line thickness than Cloisite 25A nanoclay or Cloisite 15A nanoclay. The bond line thickness of Cloisite 15A and Cloisite 25A nanoclays are essentially the same.

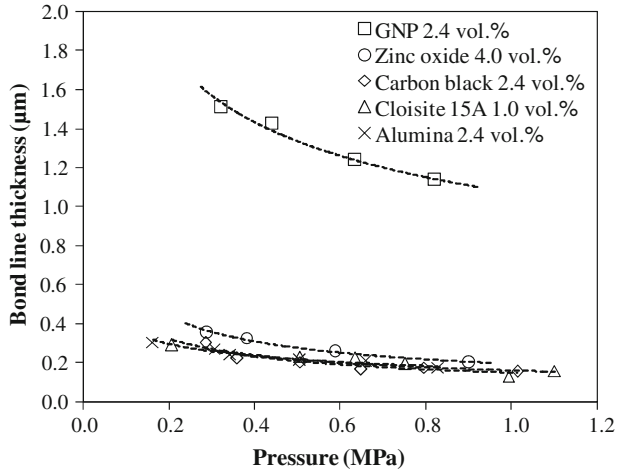

Fig. 9. Dependence of the bond line thickness on the pressure of various pastes. □: 2.4 vol.% GNP[15]; ○: 4.0 vol.% silane treated fumed zinc oxide (Z805, Degussa AG, Hanau, Germany[17]); ◇: 2.4 vol.% carbon black (Vulcan XC72R, Cabot Corp., Billerica, MA[11]); ×: 2.4 vol.% silane treated fumed alumina (Aeroxide ALU C 805, Degussa AG, Hanau, Germany[17]); Δ: 1.0 vol.% Cloisite 15A nanoclay.

Cloisite 10A nanoclay gave the highest bond line thickness for both nanoclay contents of 3 vol.% and 5 vol.% (Fig. 8). At a nanoclay content of 5.0 vol.% (Fig. 8b), Cloisite 10A nanoclay has the highest bond line thickness, Cloisite 25A nanoclay has an intermediate thickness, and Cloisite 15A nanoclay has the smallest thickness, when compared at the same pressure. These results are consistent with the conformability results (Table IV), which indicate that Cloisite 15A nanoclay has the highest conformability, followed by Cloisite 25A nanoclay, and then Cloisite 10A nanoclay. Thus, among the nanoclay pastes, a high conformability correlates with a low bond line thickness. Table I shows that the thermal contact conductance is highest for Cloisite 15A nanoclay. Thus, a low bond line thickness is associated with a high thermal contact conductance. This means that the low bond line thickness is a cause for the high effectiveness of the Cloisite 15A nanoclay paste as a thermal interface material.

The bond line thickness is shown in Fig. 9 for nanoclay, carbon black, zinc oxide, alumina, and GNP pastes. In addition, Fig. 9 shows the effect of pressure on the bond line thickness. The pressure (0.2 MPa to 1 MPa) is in the range used in the thermal contact conductance measurement (Table I). Except for the GNP paste, the bond line thickness values of all the pastes tested are in the submicron range. These values are much lower than those of the commercial thermal interface materials.[17] For the 1 vol.% Cloisite 15A nanoclay paste, the bond line thickness is essentially equal to those of the carbon black paste and the alumina paste. The bond line thickness is slightly higher for the zinc oxide paste than for the carbon black paste or the alumina paste. Consistent with this the thermal contact conductance (for the case of smooth

surfaces) for the zinc oxide paste is lower than those of the carbon black paste or the alumina paste (Table I). Thus, the low thermal contact conductance of the zinc oxide paste for the case of smooth surfaces is attributed to the relatively large bond line thickness. The bond line thickness of GNP paste is much higher than those of the other pastes in Fig. 9, thus compromising the performance of the GNP paste as a thermal interface material for smooth surfaces (Table I).

Origin of the High Thermal Contact Conductance Provided by Nanoclay

Low bond line thickness, high conformability, and low viscosity all contribute to the high thermal contact conductance provided by nanoclay (Cloisite 15A) for smooth surfaces. Comparative evaluation of the nanoclay pastes, in addition to the carbon black, alumina, zinc oxide, and GNP pastes, shows that the small bond line thickness is the most important cause of the high performance of the nanoclay paste for smooth surfaces.

The nanoclay has a platelet shape with a thickness of 1 nm. The high aspect ratio results in preferred orientation of the nanoclay platelets in the vehicle during the compression of the nanoclay paste. As a consequence, the bond line thickness is small. GNP also has nanoplatelet morphology, but the relatively strong interlayer interaction in graphite makes it more difficult for a small bond line thickness to be obtained. In contrast, the fumed oxide and carbon black particles exhibit an aggregate structure that is related to the fusion joining of the primary particles. The aggregate structure causes the carbon black and fumed oxide pastes to be less amenable to providing a very small bond line thickness than the clay paste. This notion is consistent with the fact that the thermal contact conductance decreases with increasing pressure more significantly for nanoclay than for carbon black or alumina (Table I). It is also consistent with the fact that the nanoclay paste underperforms the carbon black, alumina or zinc oxide pastes for rough surfaces, but outperforms these other pastes for smooth surfaces; the small depth of the valleys in the surface topography in the smooth case facilitates the attainment of a small bond line thickness.

An abrupt drop in thermal conductance occurs upon the addition of 1 vol.% Cloisite 15A nanoclay to the vehicle. In contrast, the conductance is increased upon the addition of a small volume fraction of Cloisite 15A nanoclay in the smooth case (Figs. 2 and 3). This behavior is consistent with the relative importance of a small bond line thickness in the smooth case and the relative importance of the thermal conductivity in the rough case. The nanoclay is attractive in providing a small bond line thickness, but is not attractive for providing a high thermal conductivity. The viscosity is increased by the addition of 0.6 vol.% Cloisite 15A nanoclay to the vehicle (Fig. 5) and this increase is not advantageous for the smooth case, but the viscosity apparently plays a less important role than the bond line thickness.

In general, a small bond line thickness is valuable, although a high thermal conductivity helps. In spite of the relatively high thermal conductivity, GNP is inferior to nanoclay as a thermal interface material, due to the relatively large bond line thickness. As another example, the thermal contact conductance of the Shin-Etsu paste is only $(19.9 \pm 0.3) \times 10^4$ W/m^2 K for smooth surfaces at 0.46 MPa (Table I), although it has a high thermal conductivity (6.0 W/mK, according to Shin-Etsu literature). This relatively low value of the conductance (Table I) is because of the large bond line thickness of 27 ± 5 μm.[17]

The thermal contact conductance differences among Cloisite 10A, Cloisite 25A, and Cloisite 15A nanoclays are believed to be mainly caused by the differences in the surface condition. Since Cloisite 15A nanoclay is more hydrophobic, it can be dispersed better in the organic vehicle, resulting in smaller agglomerate size, smaller floc size, greater conformability, and hence smaller bond line thickness.

In spite of the above arguments, a small bond line thickness is inadequate for explaining the exceptional performance of the nanoclay paste, since alumina and carbon black pastes have similarly low values of the bond line thickness (Fig. 9). Thus, the origin of the exceptional performance of nanoclay is not totally clear.

CONCLUSION

A thermal paste in the form of a polyol ester vehicle containing 0.6 vol.% nanoclay is an effective thermal interface material. Among Cloisite 15A, 25A, and 10A nanoclays, Cloisite 15A is the most effective, due to the high conformability and the consequently small bond line thickness. This preferred type of nanoclay contains a quarternary ammonium salt organic modifer (dimethyl dehydrogenated tallow) at 125 meq/100 g clay, with exfoliation conducted by using the vehicle. When it is used between copper surfaces that are smooth (0.009 μm), with a pressure of 0.69 MPa, the thermal contact conductance reaches 40×10^4 W/m^2 K, in contrast to the corresponding values of 28×10^4 W/m^2 K, 28×10^4 W/m^2 K, 25×10^4 W/m^2 K, and 24×10^4 W/m^2 K previously reported for carbon black paste, silane treated fumed alumina paste, silane treated fumed zinc oxide paste, and graphite nanoplatelet paste, respectively. Among all these fillers, graphite nanoplatelet is the least effective for smooth surfaces, in spite of its highest thermal conductivity, which makes it slightly more effective than any of the other fillers studied for the case of rough surfaces. When the nanoclay paste of the preferred composition is used between rough copper surfaces (12 μm), the conductance is below

the values attained by any of the other pastes studied. The superiority of the nanoclay paste for smooth surfaces is attributed to the small bond line thickness (less than 1 μm). The inferiority of the nanoclay paste for rough surfaces is attributed to the low thermal conductivity.

For the nanoclay paste of the preferred composition, the thermal contact conductance for the smooth case increases from 31×10^4 W/m^2 K to 40×10^4 W/m^2 K upon increasing the pressure from 0.46 MPa to 0.69 MPa. This pressure dependence is stronger than that of any of the other pastes studied.

For the preferred Cloisite 15A nanoclay, the optimum volume fraction is 0.6% for smooth surfaces; this volume fraction gives slightly higher effectiveness than the volume fractions of 0.3% or 1.0%. For rough surfaces, the optimum volume fraction is 2.0 vol.%, with 1.5 vol.% and 3.0 vol.% being slightly less effective.

REFERENCES

1. E.G. Wolff and D.A. Schneider, *Int. J. Heat Mass Tranfer.* 41, 3469 (1998). doi:10.1016/S0017-9310(98)00067-2.
2. T. Ouellette and M. de Sorgo, *Proc. Power Electron. Des. Conf.* (Power Sources Users Conference, Cerritos, CA, 1985), p. 134.
3. M.R. Vogel, *Proc. Int. Intersociety Electron. Packag. Conf.*, Vol. 10-2 (New York, NY: American Society of Mechanical Engineers, 1995), p. 989.
4. V. Sartre and M. Lallemand, *Appl. Therm. Eng.* 21, 221 (2001). doi:10.1016/S1359-4311(00)00034-X.
5. M. Grujicic, C.L. Zhao, and E.C. Dusel, *Appl. Surf. Sci.* 246, 290 (2005). doi:10.1016/j.apsusc.2004.11.030.
6. D.D.L. Chung, *J. Mater. Eng. Perform.* 10, 56 (2001). doi:10.1361/105994901770345358.
7. D.D.L. Chung, *Adv. Microelectron.* 33, 8 (2006).
8. L. Maguire, M. Behnia, and G.L. Morrison, *Microelectron. Reliab.* 45, 711 (2005). doi:10.1016/j.microrel.2004.10.030.
9. Y. Xu, X. Luo, and D.D.L. Chung, *J. Electron. Packag.* 124, 188 (2002). doi:10.1115/1.1477191.
10. C.-K. Leong and D.D.L. Chung, *Carbon* 41, 2459 (2003). doi:10.1016/S0008-6223(03)00247-1.
11. C.-K. Leong and D.D.L. Chung, *Carbon* 42, 2323 (2004). doi:10.1016/j.carbon.2004.05.013.
12. C.-K. Leong, Y. Aoyagi, and D.D.L. Chung, *J. Electron. Mater.* 34, 1336 (2005). doi:10.1007/s11664-005-0259-2.
13. C.-K. Leong, Y. Aoyagi, and D.D.L. Chung, *Carbon* 44, 435 (2006). doi:10.1016/j.carbon.2005.09.002.
14. T.A. Howe, C.-K. Leong, and D.D.L. Chung, *J. Electron. Mater.* 35, 1628 (2006). doi:10.1007/s11664-006-0209-7.
15. C. Lin and D.D.L. Chung, *Carbon* (in press).
16. Y. Xu, C.-K. Leong, and D.D.L. Chung, *J. Electron. Mater.* 36, 1181 (2007). doi:10.1007/s11664-007-0188-3.
17. C. Lin and D.D.L. Chung, *J. Mater. Sci.* 42, 9245 (2007). doi:10.1007/s10853-007-1911-4.
18. Y. Aoyagi and D.D.L. Chung, *J. Mater. Sci.* 42, 2358 (2007). doi:10.1007/s10853-007-1600-3.
19. C. Lin, T.A. Howe, and D.D.L. Chung, *J. Electron. Mater.* 36, 659 (2007). doi:10.1007/s11664-007-0116-6.
20. A. Yu, P. Ramesh, M.E. Itkis, E. Bekyarova, and R.C. Haddon, *J. Phys. Chem. C* 111, 7565 (2007). doi:10.1021/jp071761s.
21. S. Mohanty and S.K. Nayak, *Polym. Compos.* 28, 153 (2007). doi:10.1002/pc.20284.
22. M. McAlpine, N.E. Hudson, J.J. Liggat, R.A. Pethrick, D. Pugh, and I. Rhoney, *J. Appl. Polym. Sci.* 99, 2614 (2006). doi:10.1002/app.22582.
23. H. Xia and M. Song, *Polym. Int.* 55, 229 (2006). doi:10.1002/pi.1948.
24. R. Krishnamoorthi and R.A. Vaia, eds., *Polymer Nanocomposites: Synthesis, Characterization, and Modeling* (Washington DC: American Chemical Society, 2002), Distributed by Oxford University Press.
25. E. Chen, *Br. Ceram. Trans.* 103, 241 (2004). doi:10.1179/096797804X4592.
26. J.C. Matayabas Jr. and P.A. Koning, U.S. patent 6,924,027 (2005).
27. J. Matayabas Jr., PCT Int. Appl. WO 2005031864 (2005).
28. D. Burgentzlé, J. Duchet, J.F.A. Gérard, A. Jupinb, and B. Fillon, *J. Colloid Interface Sci.* 278, 26 (2004). doi:10.1016/j.jcis.2004.05.015.
29. V.E. Yudina, G.M. Divouxb, J.U. Otaigbeb, and V.M. Svetlichnyi, *Polymer (Guildf.)* 46, 10866 (2005). doi:10.1016/j.polymer.2005.08.087.
30. T.T. Chasteka, A. Steina, and C. Macosko, *Polymer (Guildf.)* 46, 4431 (2005). doi:10.1016/j.polymer.2005.02.062.
31. D. Burgentzlé, J. Duchet, J.F. Gérard, A. Jupin, and B. Fillon, *J. Colloid Interface Sci.* 278, 26 (2004). doi:10.1016/j.jcis.2004.05.015.
32. A.S.T.M. Standard, D 2196, Standard Test Methods for Rheological Properties of Non-Newtonian Materials by Rotational (Brookfield Type) Viscometer.
33. R.G. de Kretser, P.J. Scales, and D.V. Boger, *Colloids Surf.* 137, 307 (1998). doi:10.1016/S0927-7757(97)00372-5.
34. A.R. Horrocks, J. Mwila, M. Miraftab, M. Liu, and S.S. Chohan, *Polym. Degrad. Stabil.* 65, 25 (1999). doi:10.1016/S0141-3910(98)00213-4.
35. http://www.reade.com/Products/Carbons/Carbon-Black.html.
36. L.C. Sima, S.R. Ramanana, H. Ismaila, K.N. Seetharamub, and T.J. Gohc, *Thermochim. Acta* 430, 155 (2005). doi:10.1016/j.tca.2004.12.024.
37. W.M. Rohsenow, J.P. Hartnett, and Y.I. Cho, *Handbook of Heat Transfer*, 3rd ed. (McGraw-Hill Companies, Inc., 1998), p. 2.67.
38. H. Huang, C. Liu, Y. Wu, and S. Fan, *Adv. Mater.* 17, 1652 (2005). doi:10.1002/adma.200500467.
39. P.K. Schelling, L. Shi, and K.E. Goodson, *Mater. Today* 8, 30 (2005). doi:10.1016/S1369-7021(05)70935-4.
40. http://www.nanoclay.com/selection_chart.asp.
41. R.G. Larson, *The Structure and Rheology of Complex Fluids (Topics in Chemical Engineering)* (USA: Oxford University Press, 1998), pp. 324–355.